Detection of U-87 Tumor Cells by RGD-Functionalized/Gd-Containing Giant Unilamellar Vesicles in Magnetization Transfer Contrast Magnetic Resonance Images

Detection of U-87 tumor cells by RGD-functionalized/ Gd-containing Giant Unilamellar Vesicles (Gd-GUVs) in Magnetization Transfer Contrast (MTC)-MR images

Giuseppe Ferrauto[1,*], Martina Tripepi[1], Enza Di Gregorio[1], Valeria Bitonto[1], Silvio Aime[1] and Daniela Delli Castelli[1]

[1]Molecular Imaging Center, Department of Molecular Biotechnology and Health Sciences, University of Torino (IT)

* Corresponding author:
Ferrauto Giuseppe, PhD
Molecular Imaging Center, Department of Molecular Biotechnology and Health Sciences
University of Torino.
Via Nizza 52, 10126, Torino (It)

Abstract

Objectives: The targeting of tumor cells and their visualization with MRI is an important task in biomedicine. The low sensitivity of this technique is a significant drawback, and one that may hamper the detection of the imaging reporters used.

To overcome this sensitivity issue, this work explores the synergy between two strategies: *i*) RGD-functionalized Giant Unilamellar Vesicles (GUVs) loaded with Gd-complexes to accumulate large amounts of MRI contrast agent at the targeting site; and *ii*) the use of Magnetization Transfer Contrast (MTC), which is a sensitive MRI technique for the detection of Gd-complexes in the tumor region.

Materials and Methods: GUVs were prepared using the gentle swelling method, and the cyclic RGD targeting moiety was introduced onto the external membrane. Paramagnetic Gd-containing complexes were both part of the vesicle membranes and were the payload within the inner aqueous cavity together with the fluorescent probe, rhodamine. GUVs that were loaded with the imaging reporters, but devoid of the RGD targeting moiety, were used as controls. U-87 MG human glioblastoma cells, which are known to overexpress the targets for RGD moieties, were used. In the *in-vivo* experiments, U-87 MG cells were subcutaneously injected into *nu/nu* mice and the generated tumors were imaged using MRI, 15 days after cell administration. MRI was carried out at 7 T, and

T_{2W}, T_{1W} and MTC/Z-spectra were acquired. Confocal microscopy images and ICP-MS were used for result validation.

Results: *In-vitro* results show that RGD GUVs specifically bind to U-87 MG cells. Microscopy demonstrates that: *i)* RGD GUVs were anchored onto the external surface of the tumor cells without any internalization; *ii)* a low number of GUVs per cell were clustered at specific regions; *iii)* there is no evidence for macrophage uptake or cell toxicity. The MRI of cell pellets after incubation with RGD GUVs and untargeted ctrl-GUVs was performed. No difference in T_1 signal was detected, whereas a 15% difference in MT contrast is present between the RGD-GUV-treated cells and the ctrl-GUV-treated cells.

MR images of tumor-bearing mice were acquired before and after (t=0, 4 h and 24 h) the administration of RGD GUVs and ctrl-GUVs. A roughly 16% MTC difference between the two groups was observed after 4 h. Immunofluorescence analyses and ICP-MS analyses (for Gd-detection) of the explanted tumors confirmed the specific accumulation of RGD GUVs in the tumor region.

Conclusions: RGD GUVs appear to be interesting carriers that can facilitate the specific accumulation of MRI contrast agents at the tumor region. However, the concentration achieved is still below the threshold needed for T_{1w}-MRI visualization. Conversely, MTC proved to be sufficiently sensitive for the visualization of detectable contrast between pre- and post-targeting images.

Keywords

Gd-contrast agents; Giant liposomes; Imaging agents; Magnetization Transfer Contrast (MTC); Magnetic Resonance Imaging (MRI); T_1 agents; RGD tumor targeting.

Introduction

Cancer is currently considered to be one of the most dangerous threats to human health, with more than 18 million new cases and 9 million deaths per year worldwide.[1] Early diagnosis and personalized medicine are currently considered to be the main tools for oncologists in the battle to fight cancer.

Magnetic Resonance Imaging (MRI) is one of the most powerful of the available diagnostic techniques for the *in-vivo* imaging of cancer because of its high spatial resolution (in the order of μm), the possibility of visualizing soft deep tissues and the absence of ionizing radiation.[2] The use of exogenous Gd-based contrast agents (GBCAs) often enhances the potential of the technique as it adds physio-pathological information to the superb spatial resolution that can be obtained from MR images.[3-7] Unfortunately, the intrinsically low sensitivity of MRI requires the presence of relatively high amounts of GBCAs, making their use in molecular-imaging protocols problematic. It was established quite early in the technique's lifetime that the accumulation of *ca*. 10^8 gadolinium atoms per cell is required to reach the MRI detection threshold.[8]

Caution in the use of GBCAs has recently been advised. Although they are highly water soluble complexes that have been chemically designed for complete elimination from the body after intravenous administration, it has been widely demonstrated that the metal can accumulate in many organs (*e.g.* brain, kidney, liver, muscles, etc.).[9-14]

One of the most important goals, that of early diagnosis, can therefore be achieved by developing GBCAs that can specifically accumulate at the pathological tissue, via binding to epitopes that identify the tumor cells, even when the disease is at the preliminary stages. This can reduce the dose of GBCAs and improve the diagnostic potential of MRI. However, this task is often hampered by the small number of targeting sites that allow differentiation between healthy and tumor tissues.[15]

The issue of overcoming the sensitivity threshold that is associated with the presence of a limited number of targeted epitopes may be tackled using the synergic combination of two approaches: *i)* the

use of targeted nano- or micro-sized systems that carry a high number of GBCAs;[16-20] and *ii)* the use of highly sensitive MRI procedures/sequences for detecting those same GBCAs.[21]

A large *portfolio* of targeted nano- or micro-sized systems that can carry MRI CAs is available.[16-20] In general, such systems have to display: *i)* high biocompatibility; *ii)* a long *in-vivo* half-life so that as many targets as possible can be reached; and *iii)* the capacity to carry a high payload of GBCAs. Of the available nano-/micro-systems, liposomes are largely considered to be the candidates of choice, as seen in several successful cases reported in pre-clinical studies.[16-20] The use of micro-sized liposomes (Giant Unilamellar Vesicles, GUVs, mean diameter in the micrometric range) appears to represent a further step forward, both in terms of the delivery of higher amounts of GBCAs and their particular binding to extracellular epitopes, as their large size hampers cell internalization and uptake by macrophages.[22,23] GUVs can be easily prepared and characterized and, recently, have been formulated with Ln-complexes either loaded into their inner cavity (hydrophilic complexes) or incorporated into the phospholipidic membrane (hydrophobic or amphiphilic systems).[22-24]

Both linear and macrocyclic Gd-complexes are currently being used as CAs in clinical MRI applications. Their presence is detected by acquiring T_{1W}-MR images, *i.e.* by exploiting the relaxation enhancement they yield on bulk water protons (longitudinal relaxation time, T_1). The detection of GBCAs via T_1 contrast requires the accumulation of high amounts of Gd-complexes in the voxels of interest (of the order of 5- 50 μM). This concentration is not easily attainable in targeting MRI experiments.[25]

Some years ago, we reported the use of Magnetization Transfer Contrast (MTC) as a means of improving the MRI detection of T_1 relaxation agents.[20]

The method is based on the T_1 dependence of MT contrast, and we discovered that tiny amounts of GBCAs, not enough to affect the T_{1w} images, are sufficient to affect the MTC readout.

Magnetization Transfer Contrast (MTC) is a MRI procedure that has been shown to be particularly useful in several clinical applications.[26-29]

It is based on the radiofrequency saturation of resonances of protons that belong to immobilized, semi-solid macromolecules (*e.g.* proteins in the cytoskeleton or bound to biomembranes) and of the water molecules that are tightly bound to them, which are not detectable in NMR spectra because of their very short T_2 relaxation times. Upon radiofrequency irradiation (at a chemical shift that is far from *bulk* water resonance), the saturated protons may enter the free bulk water proton pool, and thus transfer their saturated magnetization to the free water protons.

The magnetization transfer lead to a decrease of the MR signal and consequently to the generation of contrast due to the difference between the signal acquired with and without the saturation pulse. The MT amount is directly proportional to the longitudinal relaxation time (T_1) of the *bulk* water protons (*i.e.* the longer the T_1 the higher is the associated MTC effect) (**Chart S1**). [20] Thus, it is expected that the presence of paramagnetic GBCAs (causing a reduction of T_1) would result in a decrease of the MT amount. The herein reported contrast relies in the difference between MR signals acquired with a MT based protocol before and after GBCAS administration. In particular, the MR signal increases after GBCAs administration. This behavior was earlier reported in cells and the sensitivity showed to be higher with respect to conventional T_{1w} contrast. [20] Starting from the above reported considerations, herein we investigated the synergic advantage of using Gd-containing-GUVs and MTC-MRI methodology for targeting tumor cells.

RGD GUVs loaded with Gd complexes, both in the membranes and in the inner cavity, able to bind integrins, were synthesized for this purpose. This study deals with *in-vitro* and *in-vivo* investigations, using U-87 MG human glioblastoma cells, which are known to overexpress beta-integrins.

Materials and Methods

Chemicals

ProHance (Gadoteridol, Gd-HPDO3A) was a gift provided by Bracco Imaging S.p.A.[30]

1,2-dipalmitoyl-*sn*-glycero-3-phosphocholine (DPPC), 1,2-distearoyl-*sn*-glycero-3-phosphoethanolamine-N-[methoxy(polyethylene glycol)-2000] (ammonium salt) (DSPE-

mPEG2000), 1,2-dioleoyl-*sn*-glycero-3-phosphoethanolamine-N-(lissamine rhodamine B sulfonyl) (ammonium salt) (Liss Rhod PE) and 1,2-distearoyl-*sn*-glycero-3-phosphoethanolamine-N-[maleimide(polyethylene glycol)-2000] (ammonium salt) were purchased from Avanti Polar Lipids Inc. (Chemical structures in **Fig.S1**).

A Gd-amphiphilic complex, Gd(III)-DOTAMA $(C18)_2$,[31] was synthesized as previously reported (Chemical structures in **Fig.S2**). The presence of free Gd-ions was checked using the Orange xylenol procedure and was lower than 0.3% *mol/mol*. [32] The exact Gd-complex concentration was checked using a relaxometric approach, as previously reported.

Cyclo(-Arg-Gly-Asp-D-Phe-Cys) acetate salt, hereinafter indicated as c(RGDfC), was purchased from Bachem AG (Bubendorf, De) (Chemical structures in **Fig.S3**).

Fluorescein-Isothiocyanate-labelled Phalloidin, from *Amanita phalloides*, hereinafter indicated as Phalloidin-FITC, was purchased from Sigma-Aldrich Co. LLC and used without further purification.

Sodium chloride, sodium acetate, HEPES (4-(2-hydroxyethyl)-1-piperazineethane-sulfonic acid), sodium hydroxide, hydrochloric acid, nitric acid, chloroform and all other chemicals were acquired from Sigma-Aldrich Co. LLC and used without further purification.

Giant liposome (GUVs) preparation

Giant liposomes were prepared according to a procedure reported in the literature with modifications.[23,33]

Membranes were prepared using the following formulations:

- RGD-Gd GUVs: DPPC (86.95%), Gd-amphiphilic complex (10%), DSPE-PEG2000Malemide (3%), 18:1 Liss Rhod PE (0.05%) (*moles %*);
- ctrl-Gd GUVs: DPPC (86.95%), Gd-amphiphilic complex (10%), DSPE-mPEG2000 (3%) 18:1 Liss Rhod (0.05%) (*moles %*).

Briefly, the desired blend of phospholipids is dried until a film is formed at the bottom of a flask. The hydration solution was then added. 40 mM Gd-HPDO3A in HEPES/NaCl buffer (3.8 mM HEPES,

0.15 M NaCl, pH 7.2±0.1) was used for both GUV formulations. The system was left for 2 h at 60°C without any mechanical stress to allow the vesicles to close and internalize the hydration solution within the inner cavity. The GUVs were then pelleted by centrifugation, washed with fresh HEPES/NaCl buffer and purified from any non-internalized hydration solution, impurities or (if present) small liposome populations that may have remained in the surnatant.

GUV size was determined using confocal fluorescence microscopy on a fluorescent formulation (0.05% Liss Rhod PE in the membrane and 20 μM 5(6)-carboxyfluorescein in the cavity). Z-stack images were acquired in order to center every vesicle in its main diameter in order to be suitably manually measured. Dynamic Light Scattering (DLS) measurements confirmed the absence of liposome populations of between 50 nm and 800 nm.

The molar concentration of small and giant vesicles was evaluated using the reported formula, with modifications (1,2):[34]

$$[Liposomes] = \frac{[Gd]_i \times 1L}{V_i \times [Gd]_{intralipo}} = \frac{[Gd]_i \times 1L}{\frac{4}{5}\pi^3 \times [Gd]_{intralipo}} \quad (1)$$

where

$$[Gd]_i = [Gd]_{TOT} - [Gd]_m \quad (2)$$

$[Gd]_{TOT}$ is determined *via* the acidic digestion of the sample and quantification of Gd^{3+} by ICP-MS,

$[Gd]_m$ is the amount of Gd present in the membrane,

r is the radius of the vesicle,

$[Gd]_{intralipo}$ is assumed to be the same as that of the hydration solution.

c(RGDfC) was attached by chemical ligation.[35] Briefly, GUVs were suspended in HEPES/NaCl buffer and centrifuged to obtain pellets. They were then suspended in 0.15 M sodium acetate buffer (pH=6.8). An excess of c(RGDfC) was then slowly added to the GUVs suspension, which was gently agitated for 4 h, under a N_2 atmosphere. Finally, GUVs were centrifuged and washed two times with fresh HEPES/NaCl buffer.

Cell cultures

Human glioblastoma U-87 MG cells were used for experiments (ATCC n° HTB-14). They were cultured in Eagle Minimum Essential Medium (EMEM) supplemented with 10% fetal bovine serum (FBS), 2 mM glutamine, 100 U/mL penicillin and 100 μg/mL streptomycin. Cells were seeded in 75-cm^2 flasks at a density of ca. 2×104 cells/cm^2 in a humidified 5% CO_2 incubator at 37 °C. At confluence, they were detached by adding 1 mL of a Trypsin-EDTA solution (0.25 % (w/v) Trypsin-0.53 mM EDTA).

Cells were negative for mycoplasma, as tested using the MycoAlert™ Mycoplasma Detection Kit (Lonza Sales AG-EuroClone S.p.A., Milano, It).

All cell media and supplements were purchased from Lonza Sales AG-EuroClone S.p.A. (Milano, It).

Cytotoxicity assay

Preliminary tests to assess the toxicity of GUVs were carried out using U-87 MG cancer cells in the MTT assay.[36] Cells were seeded into 96-well tissue culture plates (10^4 cells per plate) 24h before the experiment. They were then incubated with fresh complete medium in the presence of RGD-Gd GUVs or ctrl-Gd–GUVs (concentration of vesicles is 0÷20 pM).

After incubation, the medium was removed, the cells were washed and re-incubated in the presence of fresh medium supplemented with 0.5 mg/mL MTT (Thiazolyl Blue Tetrazolium Bromide, Sigma Aldrich) for 4 h in a humidified 5% CO_2 incubator at 37°C. Then, the MTT solution was removed and the plates were filled with DMSO (0.1 mL for plate) for ½ h at room temperature, under gentle agitation, to allow the formazan crystals to solubilize. The absorbance of the resulting colored solutions was quantified using a 96-multiwell iMark Bio-Rad microplate Reader (λ = 570 nm). The percentage of viable cells was calculated on the basis of the control blank cells using the following formula (3):

$$Viable\ cells\ \% = \frac{Abs-T}{Abs-cnt} \times 100 \qquad (3)$$

Where Abs-T is the mean absorbance of the treated cells and Abs-cnt is the mean absorbance of the control untreated cells (after subtraction of the absorption of empty plates as background). Cell experiments were repeated in triplicate and the data are reported as mean ± standard deviation. The blank was repeated 10 times.

Cell labelling

Human glioblastoma U-87 MG cells (8x105) were seeded in 6-cm Petri dishes containing 3 mL of complete EMEM medium and were placed in a humidified 5% CO_2 incubator at 37°C. The day after, when cells had reached *ca.* 70-80% confluence, they were incubated in fresh medium in the presence of either ctrl-Gd GUVs or RGD-Gd GUVs (concentration of vesicles is ca. 4 pM), for 30 min at 37°C. The cells were then washed 3-times with fresh PBS and detached using a non-enzymatic cell dissociation solution (Lonza Sales AG-EuroClone S.p.A., Milano, It). Finally, cells were loaded into glass capillaries and centrifuged at 1200 rpm for 5 min to give pellets for MRI acquisition.

Animals

The *in-vivo* experiments were performed on male athymic nude mice (Fox 1 nu/nu, Envigo) of 7-8 weeks of age and a weight of 21±2 g. The mice were kept in standard housing with standard rodent chow, water available *ad libitum* and a 12 h light/dark cycle.

Experiments were performed according to the Amsterdam Protocol on Animal Protection, in conformity with institutional guidelines that are in compliance with national laws (D.L.vo 116/92, D.L.vo 26/2014 and following additions) and international laws and policies (2010/63/EU, EEC Council Directive 86/609, OJL 358, Dec 1987, NIH Guide for the Care and Use of Laboratory Animals, U.S. National Research Council, 1996).

For tumor-model preparation, mice were anesthetized *via* an intramuscular injection of tiletamine/zolazepam (Zoletil 100; Virbac, Milan, Italy) 20 mg/kg plus xylazine (Rompun; Bayer, Milan, Italy) 5 mg/kg using a 27-G syringe. *Ca.* 1x106 human glioblastoma U-87 MG cells were

suspended in 0.1 mL of PBS and subcutaneously injected into each leg of 8-week-old male mice (N=6, a low animal number in agreement with the 3R principles for the use of animals). Two tumors were implanted into each mouse, to double the number of analyzed tumors.

Animals were monitored by caliper weekly for changes in tumor size. MRI was performed 15 days after tumor-cell implantation when the mean tumor volume was 180±30 mm^3.

For the MRI experiments, mice were anesthetized *via* the intramuscular injection of tiletamine/zolazepam (Zoletil 100; Virbac, Milan, Italy) 20 mg/kg plus xylazine (Rompun; Bayer, Milan, Italy) 5 mg/kg using a 27-G syringe.

Permanent vein access was obtained by inserting a PE10 catheter into the tail vein (27-G needle).

The animal study protocol is reported in Fig.4A. Briefly, pre-MR images were acquired 15 days after tumor implantation. MR images were then acquired at t=0, t=4 h and t=24 h after the administration of GUVs. Mice were divided into two groups. The first group was injected with RGD-Gd GUVs (0.05 mmol Gd/kg), and the second group was injected with ctrl-Gd GUVs (0.05 mmol Gd/kg), i.e. the low range doses of current clinical GBCAs.

The injection of GUVs was performed via slow infusion (0.1 mL/min - 0.25 mL) using an infusion pump (Phd 22/2000 MRI compatible infusion/withdrawal remote programmable dual syringe pump, Harvard Apparatus), to ensure that the GUV-administration protocol was safe.

MRI acquisition and data analysis

MRI scans were acquired at 7 T on a Bruker Avance 300 spectrometer equipped with the Micro 2.5 microimaging probe. T_{1W} images were acquired using a standard MSME (multislice multiecho) sequence with the following parameters (TR = 250 ms, TE = 3.3 s, FOV = 1 cm x 1 cm, slice thickness = 1 mm, matrix size 128 x 128). T_{2W} images were acquired using a standard RARE (Rapid Acquisition with Refocused Echoes) sequence with the following parameters (TR = 4000 ms, TE = 5.5 s, FOV = 1 cm x 1 cm, slice thickness = 1 mm, RARE factor = 32, matrix size 128 x 128). T_1 values were measured using a Saturation Recovery Spin Echo sequence (TE = 3.8 ms, 10 variable TRs ranging

from 50 to 5000 ms, FOV = 1 cm x 1 cm, slice thickness = 1 mm, matrix size 128 x 128). T_2 values were measured using a MSME sequence (TR = 2000 ms, 20 variable TEs ranging from 11 to 500 ms, FOV = 1 cm x 1 cm, slice thickness = 1 mm, matrix size 128 x 128).

The T_1 contrast enhancement ($T_{1\,enh}\%$) was calculated as follows (3):

$$T_{1\,enh}\% = \frac{SI_w - SI_{w/o}}{SI_{w/o}} \times 100 \quad (3)$$

where SI_w and $SI_{w/o}$ are the normalized MR signal intensities for pellets that contained and did not contain the Gd(III)-labelled cells, respectively.

Analogously, the T_2 contrast was calculated as negative enhancement ($T_{2\,enh}\%$) using the following expression (4):

$$T_{2\,enh}\% = \frac{SI_w - SI_{w/o}}{SI_{w/o}} \times 100 \quad (4)$$

In order to evaluate the Magnetization Transfer (MT) effect, Z-spectra were acquired in the ±300 ppm range. A typical RARE spin–echo sequence with an echo time of 3 ms and a TR value of 8 s was used. An isotropic 64 × 64 acquisition matrix with FOVs of 10 x 10 mm^2, for *in-vitro* experiments, and 30 x 30 mm^2, for *in-vivo* experiments, and a slice thickness of 1 mm were used. The whole sequence was preceded by a saturation scheme consisting of a 3-sec-long continuous rectangular wave pulse at a radiofrequency B_1 intensity of either 3, 6 or 12 μT (only B_1 = 6 μT for *in-vivo* experiments). The Z-spectra were analyzed using custom-made software, and were compiled in the MATLAB platform.

The MTC effect was measured using the following equation (5):

$$MTC_{enh}\% = \frac{SI_{RGD} - SI_{ctrl}}{SI_{ctrl}} \times 100 \quad (5)$$

where SI_{RGD} an SI_{ctrl} are the normalized MR signal intensities in the Z-spectrum at 16 ppm, in the presence of RGD-Gd GUVs and ctrl-Gd GUVs respectively.

ICP-MS

After the MRI experiments were completed, the animals were sacrificed and the tumors were explanted, weighed and processed for ICP-MS analysis using reported procedures.[11] The explanted tissue was treated by adding 1 mL of concentrated HNO_3 (70%) to each sample. After the complete dissolution of the tissues, the samples were further digested using microwave heating (MicroSYNTH, Microwave labstation equipped with an optical fiber temperature control and HPR-1000/6M six position high-pressure reactor, Milestone, Bergamo, Italy). After digestion, the volume of each sample was brought to 2 mL using ultrapure water. The solutions were then filtered with a 0.45 μm filter and analyzed by ICP-MS for the quantification of Gd^{3+}, using a Thermo Scientific ELEMENT 2 ICP-MS-Finnigan, Rodano (MI). Quantification was obtained using a calibration curve that was measured using four gadolinium absorption standard solutions (Sigma-Aldrich) in the range 0.005–0.1 μg/mL. The total mass of the Gd^{3+} that was retained in each specimen was calculated with respect to the weight of the tumor tissue (as μg of Gd^{3+}/g of tissue).

Histology and confocal fluorescence microscopy

-Confocal fluorescence microscopy of U-87 MG cells incubated in the presence of Gd-GUVs: 1.5 x 10^4 U-87 MG cells were seeded into μ-Slide 8 Wells in the presence of fresh medium. One day later, they were incubated for 30 min with either Rhodamine-containing RGD-Gd GUVs or Rhodamine-containing ctrl-Gd GUVs (*ca*. 5.2 x 10^6 vesicles per plate, red). After labelling, the cells were extensively and gently washed to remove any unbound liposomes. The cells were then stained with Phalloidin-FITC (green) solution for 30 min at RT. Subsequently, the cells were washed twice with fresh PBS and observed using confocal microscopy. Z-stack images were acquired on a Leica SP8 confocal system (Leica Microsystems), in order to acquire a series of parallel images along the Z-axis that could be used to reconstruct 3D images of the GUV-labelled cells. This allowed the effective number of GUVs that were bound to cells to be assessed. The following wavelengths were considered

for microscopy: 1) λ_{ex}=545 nm, λ_{em}=567 nm for rhodamine-B; and 2) λ_{ex}=495 nm, λ_{em}=520 nm for Phalloidin-FITC. Fluorescent images were processed using ImageJ Fiji freeware software.

-Hematoxylin/Eosin and CD-31 staining: After MRI acquisition, mice were sacrificed via cervical dislocation. Cancer tissues were excised, cut along the major axis and frozen into cold isopentane (-80°C overnight). Then, 4 μm sections were prepared, using cryotome, and fixed using ice-cold acetone for 8 min. This was followed by three washings with PBS. One slice was stained with hematoxylin/eosin (H/E stain) (BioOptica) and observed under an Olympus BX41 microscope equipped with a Leica photographic system for a histological characterization of the tumor.

For CD-31 staining and confocal fluorescence microscopy,[38] slices were incubated with 10% goat serum in PBS, 1 h, RT. They were then incubated in the presence of the primary antibody (rat anti-mouse CD-31 (Invitrogen, Life technologies, 1:200 in 10% goat serum in PBS) overnight at 4°C. Slices were washed three times with PBS (5 min, under agitation) and incubated in the presence of the secondary fluorescent antibody (Alexa Fluor 488 anti-rat antibody secondary Ab, Invitrogen, Life technologies, 1:500 in PBS), for 1 h at room temperature. Subsequently, the slices were washed 3 times with PBS (5 min, under agitation), and the nuclei were stained with TO-PRO-3 via incubation with the TO-PRO-3 staining solution (Thermo-Fisher Scientific) 1:1000 in PBS, for 10 min at room temperature. After 2 washings with PBS (5 min, under agitation), the sections were mounted using ProLong Mountant (Thermo-Fisher Scientific). Sections were imaged on a Leica SP8 confocal system (Leica Microsystems). The following wavelengths were considered for microscopy: 1) λ_{ex}=545 nm, λ_{em}=567 nm for rhodamine-B of GUVs (red); 2) λ_{ex}=495 nm, λ_{em}=519 nm for CD-31 staining (green); and 3) λ_{ex}=642 nm, λ_{em}=661 nm for TO-PRO-3 nuclei staining (blue).

Statistical analysis

All data are expressed as mean ± standard deviation (N=6). The Graph-Pad Prism software was used for data analysis. The statistical analysis of the data was carried out using the unpaired two-tailed t-test. A P-value < 0.05 was taken to be statistically significant.

Results

The aim of this work is to develop a MRI methodology that can detect tumors using Gd-loaded-targeting-GUVs and the MTC-MRI modality. U-87 MG human glioblastoma cells that overexpress integrin receptors were used as the target cancer cells. For this purpose, c(RGDfC) was used as the targeting vector as it is able to bind integrin receptors. In order to target GBCAs to U-87 tumor cells, giant unilamellar vesicles were functionalized with cyclic-RGD and loaded with a amphiphilic Gd-complex in the membrane and Gd-HPDO3A in the internal aqueous cavity (RGD-Gd GUVs).

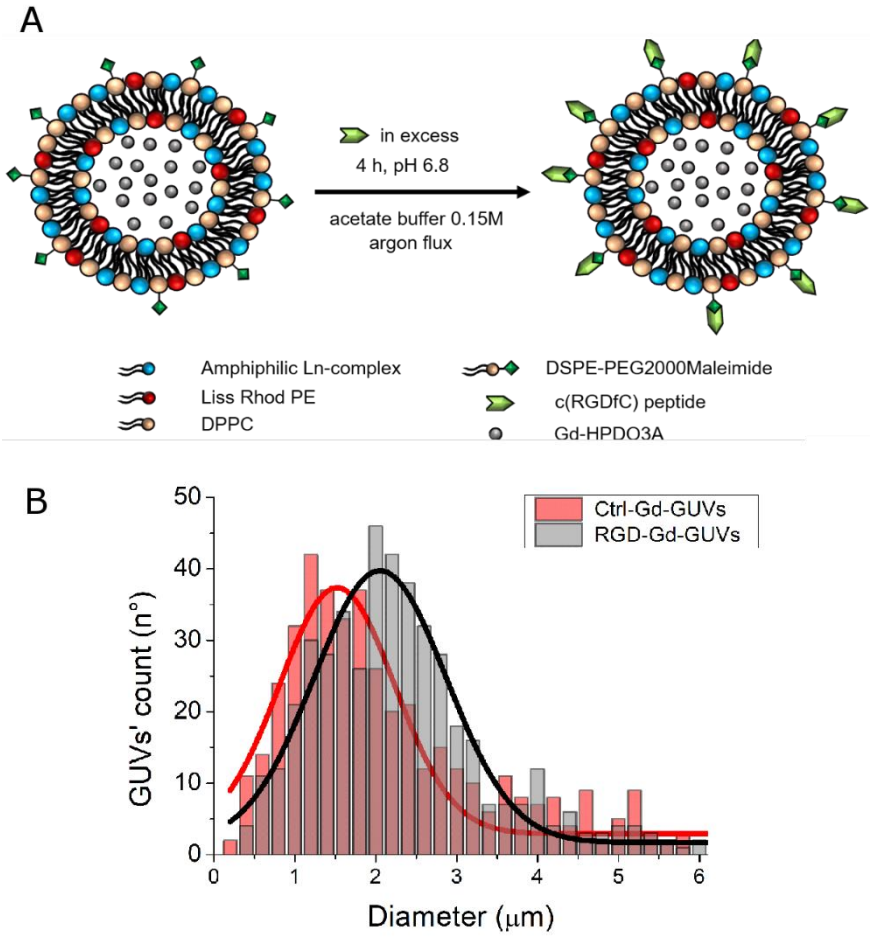

Fig.1. (A) Schematic representation of RGD-Gd-GUV formulation and the chemical addition of the targeting vector (the relative amount and size of the different chemicals is not to scale); (B) GUV diameter size distribution as assessed by confocal microscopy analysis.

Gd-HPDO3A is widely used in clinical and preclinical experiments and shows no toxicity.[39,40]

Fig.1A provides a representation of RGD-Gd GUVs. GUVs were prepared as reported in the literature,[23,33] and the c(RGDfC) peptide was attached to the DSPE-PEG2000Maleimide phospholipid component of the GUVs.[35]

Gd-GUVs *w/o* the c(RGDfC) peptide (ctrl-Gd GUVs) were prepared by incorporating DSPE-mPEG2000 phospholipids, instead of DSPE-PEG2000Maleimide, into the membrane composition, and were used as controls.

The main features of the two GUV preparations are summarized in **Table 1**. They display quite similar size (hydrodynamic diameter is 2.0 ± 0.3 and 1.5 ± 0.2 μm, for RGD-Gd GUVs and ctrl-Gd GUVs, respectively, **Fig.1B**), surface ζ-potential (-5.9 ± 0.6 mV and -2.2 ± 0.2 mV, for RGD-Gd GUVs and ctrl-Gd GUVs, respectively) and longitudinal relaxation rate (r_1 normalized for 1 mM of Gd-concentration). The relaxivities were *ca*. 5.5 $mM^{-1}s^{-1}$ and *ca.* 1.8 $mM^{-1}s^{-1}$ for RGD-Gd GUVs and ctrl-Gd GUVs at 0.5 and 7 T, respectively).

	RGD-Gd GUVs	**Ctrl-Gd GUVs**
Membrane formulation	DPPC 86.95% Amphiphilic Gd-complex 10% Liss Rhod PE 0.05% DSPE-PEG2000Maleimide 3%	DPPC 86.95% Amphiphilic Gd-complex 10% Liss Rhod PE 0.05% DSPE-mPEG2000 3%
Hydration solution	40 mM Gd-HPDO3A in HEPES/NaCl buffer (3.8 mM HEPES, 0.15 M NaCl)	40 mM Gd-HPDO3A in HEPES/NaCl buffer (3.8 mM HEPES, 0.15 M NaCl)
Hydrodynamic diameter (mean ± σ)	2.0 ± 0.3 μm	1.5 ± 0.2 μm
Surface ζ-potential (mean ± SD)	-5.9 ± 0.6 mV	-2.2 ± 0.2 mV
Longitudinal relaxation rate (r_1)	*ca.* 5.5 $mM^{-1}s^{-1}$ (at 0.5 T, 25°C) *ca.*1.8 $mM^{-1}s^{-1}$ (at 7 T, 25°C)	*ca.* 5.5 $mM^{-1}s^{-1}$ (at 0.5 T, 25°C) *ca.*1.8 $mM^{-1}s^{-1}$ (at 7 T, 25°C)

Table 1. Main features of RGD-Gd GUVs and ctrl-Gd GUVs.

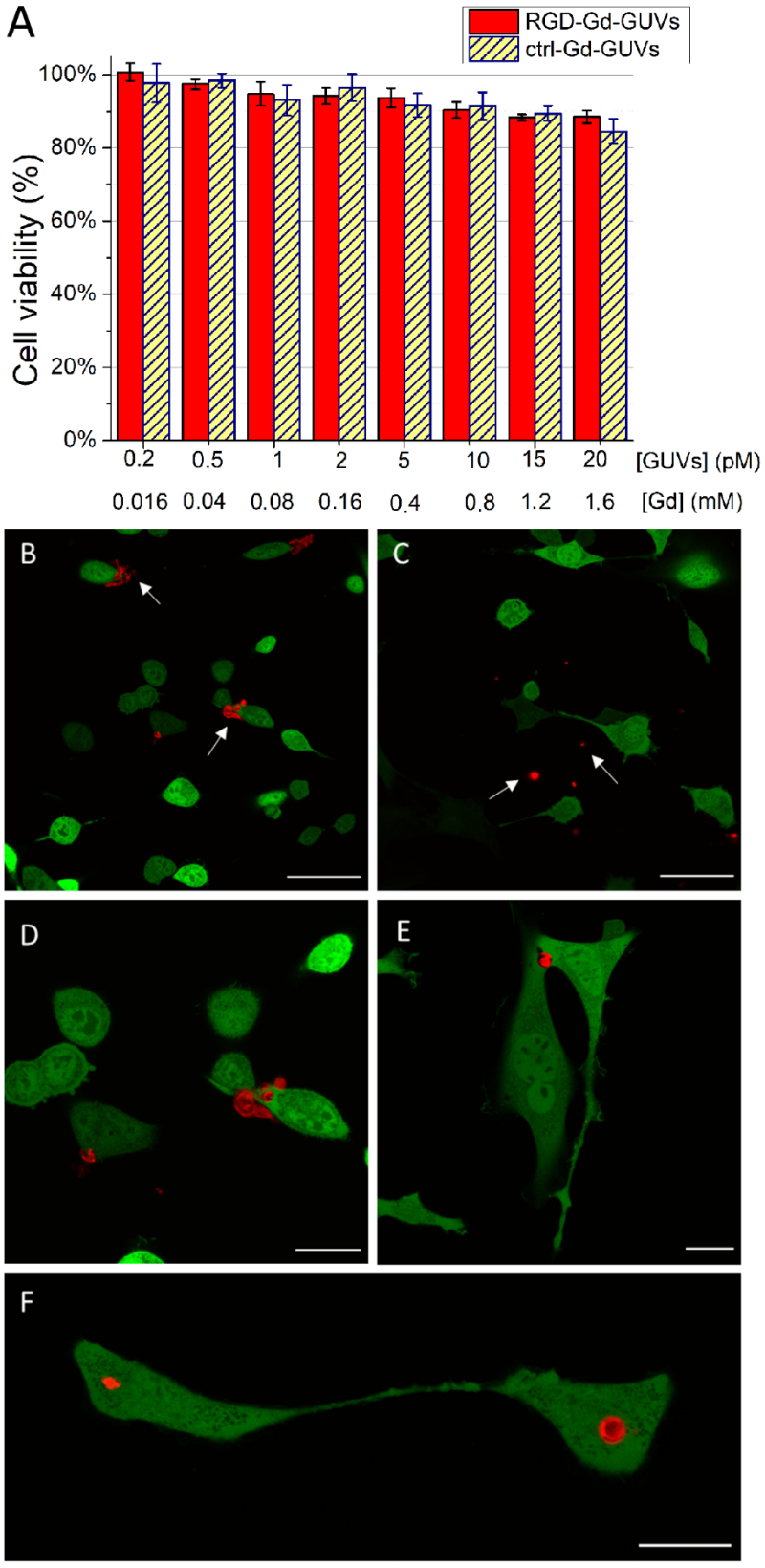

Fig.2. (A) U-87 MG cell viability upon 30 min incubation with RGD-Gd GUVs and ctrl-Gd GUVs. (B) Confocal fluorescence microscopy of live glioblastoma cells incubated in the presence of RGD-Gd GUVs, and (C) in the presence of ctrl-Gd GUVs (scale bar = 50 μm). Arrows indicate RGD-Gd GUVs and ctrl-Gd GUVs. (D, E, F) Magnification of cells incubated in the presence of RGD-Gd GUVs (*red* = rhodamine-GUVs; *green* = Phalloidin-FITC) Scale bars = 20 μm.

As the synthesized Gd-GUVs display good paramagnetic and fluorescent properties, making them suitable for MRI and fluorescence microscopy applications, they were tested for their ability to target U-87 MG cells in cultures.

Firstly, the potential cytotoxicity of the GUVs was assessed *in vitro* using a MTT cell viability test.[36] As reported in **Fig.2A**, only a small effect on glioblastoma cell viability was detected upon incubation with RGD-Gd GUVs and ctrl-Gd GUVs (cell viability is higher than 90% for [GUVs] up to *ca*. 10 pM). Moreover, no significant difference was detected in the two GUV formulations (**Fig.2A**). Overall, the observed toxicity appears to be acceptable, as expected considering the well-established tolerability of Gd-HPDO3A, which is the main GBCA in the formulations.[39,40]

Confocal microscopy images of the cells were acquired to gain further insight into the specific binding of RGD-Gd GUVs to U-87 MG cells. The cells were stained using Phalloidin-FITC (*green*). **Fig.2B** and **C** report representative images of U-87 glioblastoma cells after 30 min of incubation either in the presence of RGD-Gd GUVs (**Fig.2B**), or in the presence of ctrl-Gd GUVs (**Fig.2C**). As expected, GUVs are only bound to glioblastoma cells when the RGD moiety is present.

The binding is specific without any evidence of the GUVs or their imaging reporters being internalized within the targeted cells. Furthermore, it can be noted that only a low number of GUVs are present per cell, and that there is evident vesicle clustering in discrete cell regions (mainly in cell spines) (**Fig.2D, E** and **F** magnification of U-87 MG cells incubated in the presence of RGD-Gd GUVs). 3D fluorescence confocal microscopy reconstructions of RGD-Gd-GUV binding to U-87 MG cells have been reported in the *Supplementary information* (**Movie S1, S2** and **S3**).

Considering the positive results for the cytotoxicity and specific binding of RGD-Gd GUVs to U-87 MG cells, the *in-vitro* targeting experiments for MRI detection were carried out. For this purpose, glioblastoma cells were incubated in the presence of either RGD-Gd GUVs or ctrl-Gd GUVs (particle concentration *ca*. 1 pM) for 30 min at 37°C. Then, after extensive washing with fresh PBS buffer, the cells were detached using a non-enzymatic cell-dissociation solution, and centrifuged inside glass

capillaries to give pellets for MRI acquisition, and in order to assess T_1, T_2 and MTC responses. **Fig.3A** reports representative MRI results for the U-87 MG cell pellets (T_{2w}, T_{1w} and MTC images).

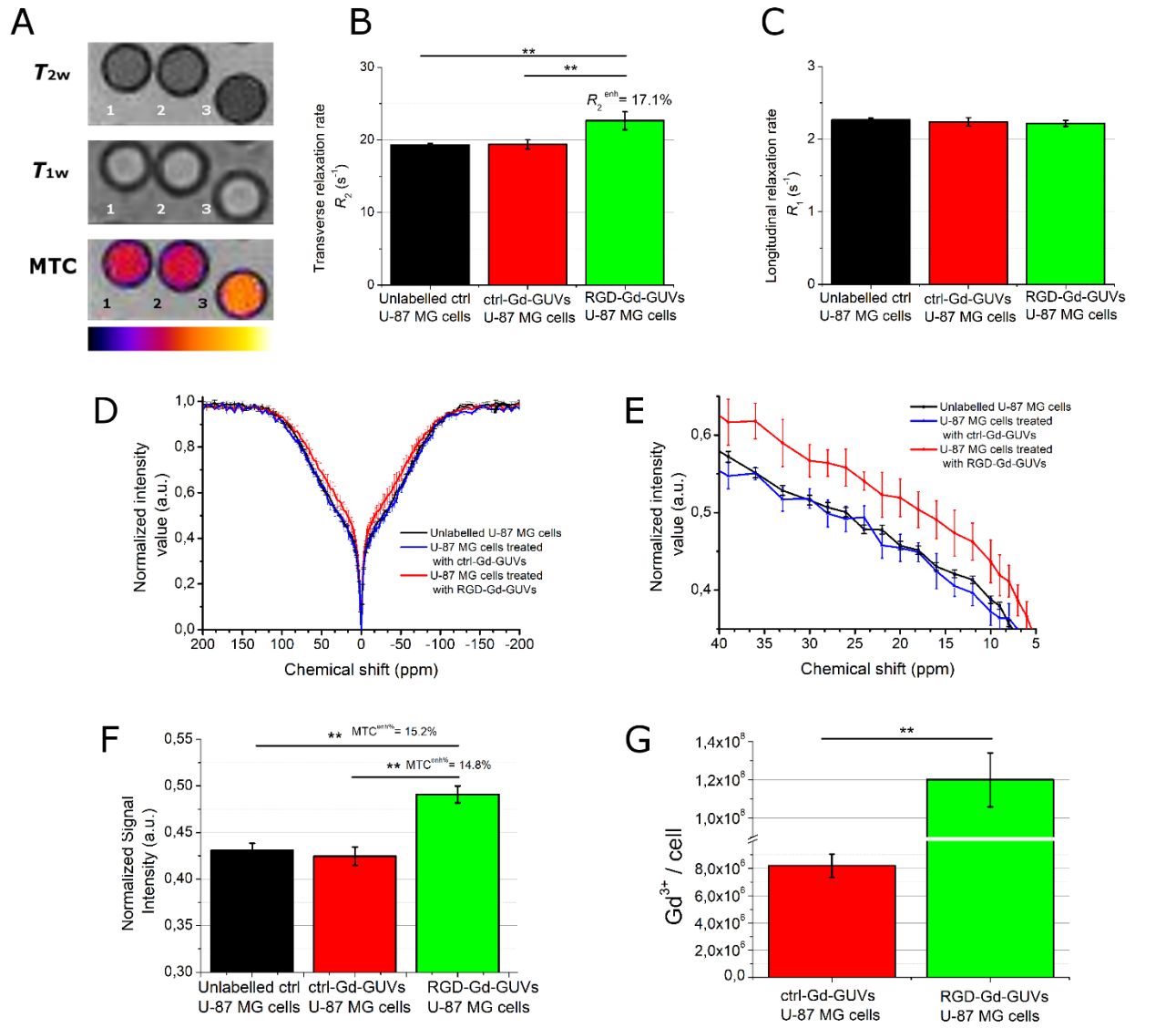

Fig.3. (A) T_{2w} (*top*), T_{1w} (*middle*) and MTC (*bottom*) MR images from representative phantoms composed of three glass capillaries filled with: 1) untreated U-87 MG cells, 2) U-87 MG cells incubated in the presence of ctrl-Gd GUVs and 3) U-87 MG cells incubated in the presence of RGD-Gd GUVs. (B) R_2 values of the three specimens. (C) R_1 values of the three specimens. (D) Z-spectra of the three specimens (B_1=6μT). (E) Magnification of the Z-spectra in the 5-40 ppm region. (F) Normalized signal intensity of the three specimens from the Z-spectra (for calculating $MTC^{enh\%}$), B_1=6μT. (G) ICP-MS quantification of Gd-content in cells.

Three specimens were considered: *i)* untreated U-87 MG cells (*negative control)*; ii) U-87 MG cells incubated in the presence of ctrl-Gd GUVs (*second negative control*); and iii) U-87 MG cells incubated in the presence of RGD-Gd GUVs. The R_2 value of the cells incubated in the presence of

ctrl-Gd GUVs was very similar to that of the specimen containing the unlabeled blank cells (19.37±0.64 *vs*. 19.31±0.19 s^{-1}, respectively) (**Fig.3B**).

Consequently, no T_2 contrast can be detected in the T_{2W}-MR images of the cells incubated in the presence of ctrl-Gd GUVs (**Fig.3A *top***). In the case of incubation in the presence of targeted RGD-Gd GUVs, only a small increase in the R_2 value was detected (*i.e.* 22.62 ± 1.22 s^{-1}, corresponding to *ca*. 17% R_2 Enhancement) (**Fig.3A**). This slight increase in the R_2 value was barely detectable as contrast in the T_{2W}-MR images (**Fig.3A *top***).

Furthermore, no differences in T_1 value nor T_1 contrast were observed in the T_{1W}-MR images (**Fig.3C**, **A *middle***). Hence, the T_1 modality cannot be considered suitable for the detection of Gd-GUV-targeted cells in the applied experimental set-up. The Z-spectra of the U-87 MG cell specimens were then acquired using several B_1 pulses.

Representative MTC results obtained with B_1= 6 μT are reported in **Fig.3A *bottom***, ***Fig.3*D** (Z-spectra), **Fig.3E** (magnification of Z-spectra) and **Fig.3F** (MTC $^{enh\%}$). A MT contrast of $MTC^{enh\%}$= 15.2±1.9 % was found for pellets of the cells treated with RGD-Gd GUVs with respect to the pellets made of untreated cells, and a of $MTC^{enh\%}$ = 14.8±2.3 % was found compared to the pellets of cells treated with ctrl-Gd GUVs. Comparable results were obtained using a B_1= 3 and 12 μT (**Fig.S4-S7**). An ICP-MS determination of the Gd content in the cell specimens upon incubation in the presence of either RGD-Gd GUVs or ctrl-Gd GUVs showed a significantly higher amount (*ca.* 15 times) of Gd in the cell specimens incubated in the presence of targeting RGD-Gd GUVs, compared to cells treated with ctrl-Gd GUVs ($1.2x10^8$ *vs.* $8.2x10^6$ Gd^{3+}/cell, respectively). Data are reported in **Fig.3G**).

U-87 MG cells were incubated in the presence of empty RGD GUVs for use as controls (*i.e.* GUVs containing RGD moiety, but with no Gd-complexes either in the membrane or inner cavity), and their Z-spectrum was quite analogous to that of the untreated cells (**Fig.S8**), indicating that the presence of Gd-complexes is needed for the MTC effect.

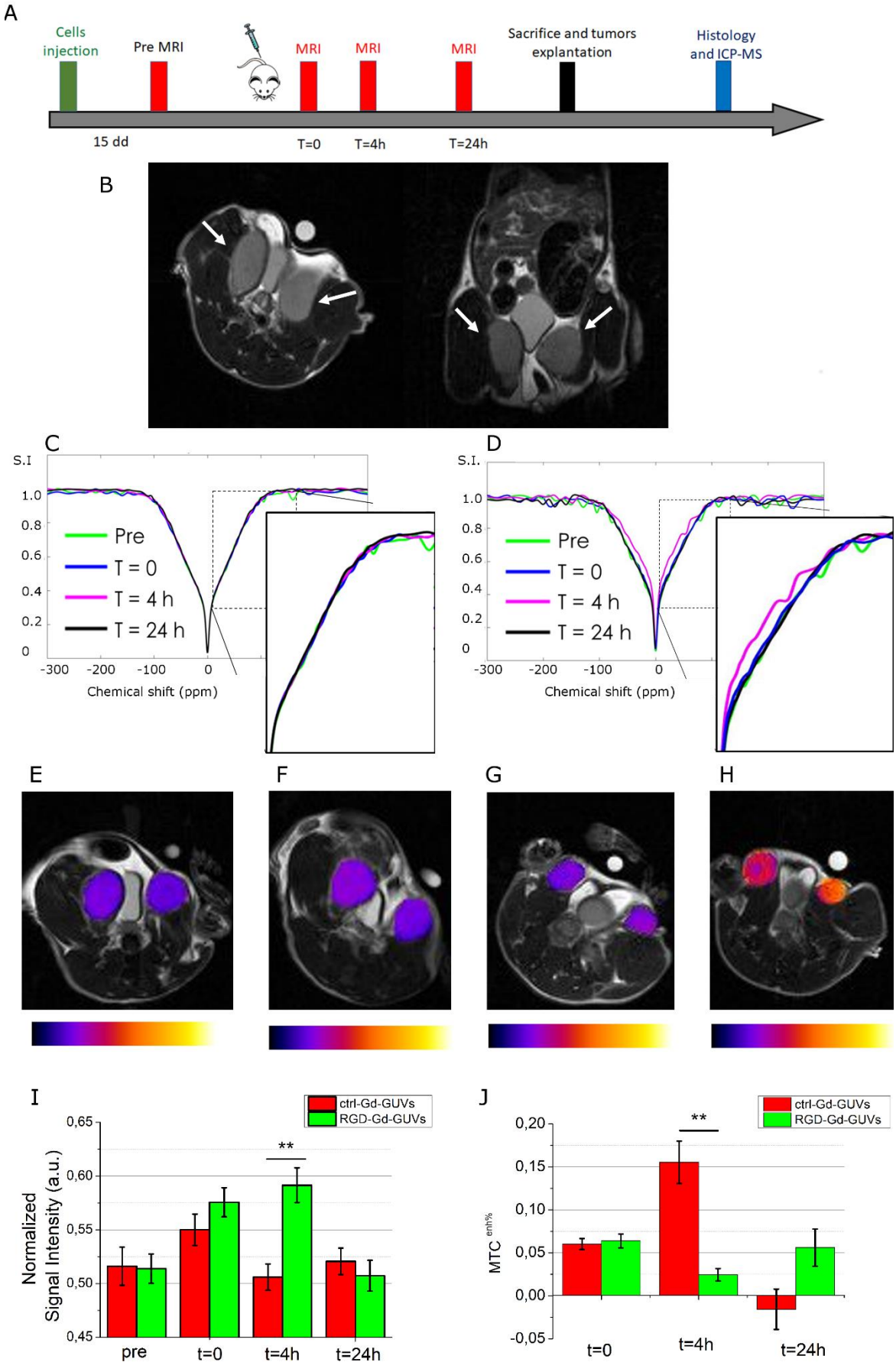
A
Cells injection
Pre MRI
MRI
MRI
MRI
Sacrifice and tumors explantation
Histology and ICP-MS
15 dd
T=0
T=4h
T=24h
B
C
S.I
1.0
0.8
0.6
0.4
0.2
0
Pre
T = 0
T = 4 h
T = 24 h
-300
-200
-100
0
Chemical shift (ppm)
D
S.I.
1.0
0.8
0.6
0.4
0.2
0
Pre
T = 0
T = 4 h
T = 24 h
-300
-200
-100
0
Chemical shift (ppm)
E
F
G
H
I
ctrl-Gd-GUVs
RGD-Gd-GUVs
Normalized Signal Intensity (a.u.)
0,65
0,60
0,55
0,50
0,45
**
pre
t=0
t=4h
t=24h
J
ctrl-Gd-GUVs
RGD-Gd-GUVs
MTC enh%
0,20
0,15
0,10
0,05
0,00
-0,05
**
t=0
t=4h
t=24h

Fig.4. (A) Experimental set-up for *in-vivo* studies. (B) Representative axial and coronal T_{2w} and T_{1w} images of tumor-bearing mice. (*White arrows indicate transplantable tumors)*. (C) Z-spectra from the tumor region before and after treatment with ctrl-Gd GUVs (t=0, 4h and 24h, Group1). (D) Z-spectra from the tumor region before and after treatment with RGD-Gd GUVs (t=0, 4h and 24h, Group2). (E) Representative MTC image of ctrl-Gd-GUV-treated mice t=0. (F) Representative MTC image of ctrl-Gd-GUV-treated mice t=4h. (G) Representative MTC image of RGD-Gd-GUV-treated mice t=0. (H) Representative MTC image of RGD-Gd-GUV-treated mice at t=4h. (I) Normalized signal intensity of tumor ROI pre- (t=0) and post-treatment (t=4h or 24h) with ctrl-Gd GUVs or RGD-Gd GUVs. (J) $MTC^{enh\%}$ of the tumor region at t=0, 4h and 24h.

The positive data obtained in cell cultures drove us to perform the *in-vivo* targeting experiments. The experimental protocol is reported in **Fig.4A**.

Representative T_{2W}- and T_{1w} MRI of tumors are reported in **Fig.4B** (*tumors are indicated by the white arrows*). The presence of the two tumor masses is clearly visible. Mice were divided into two groups. Group1 received ctrl-Gd GUVs (0.05 $mmol_{Gd}$/kg, slow infusion), whereas Group2 was treated with the same dose of RGD-Gd GUVs under analogous administration conditions. MRI was carried out before and after (t=0, 4 h and 24 h) GUV administration.

From these acquisitions, it was evident that both T_2 and T_1 contrast are not able to distinguish the tumors in Group1 mice from those of Group2 mice.

As far as the Z-spectra are concerned, no difference can be detected between pre and post ctrl-Gd-GUV administration in Group1 (**Fig.4C**). On the other hand, in the case of Group2 (administration of RGD-Gd GUVs), a clear difference in the Z-spectra is present at t=4 h post administration. At t=0 and t=24 h post injection, the Z-spectra almost completely overlap with the pre-administration ones (**Fig.4D**).

Fig.4E-H report representative MTC MR images of mice treated with either ctrl-Gd GUVs or RGD-Gd GUVs at t=0 and t=4h. The normalized signal intensities obtained from the Z-spectra of tumor ROIs are reported in **Fig.4I**. There is only a significant increase in signal, *i.e*. a reduction in the MT effect, at t=4h for the RGD-Gd-GUV-treated mice. A quantitative analysis was carried out by measuring the MTC enhancement, and the results are reported in **Fig.4J**. At t=0 there is a very small

MTC% contrast (*ca*. 5%), which is comparable for the two groups. At t=4 h the difference between the two groups is significant (16% *vs*. 2%, P-value < 0.05). At t=24 h, the MTC% of Group1 decreases and, in general, the difference between the two groups is no longer significant. The observed behavior suggests that the MTC data are indicative of the binding of RGD-Gd GUVs to glioblastoma tumor cells, with a maximum effect that corresponds to the maximum Gd accumulation (*vide infra*), at around t=4 h.

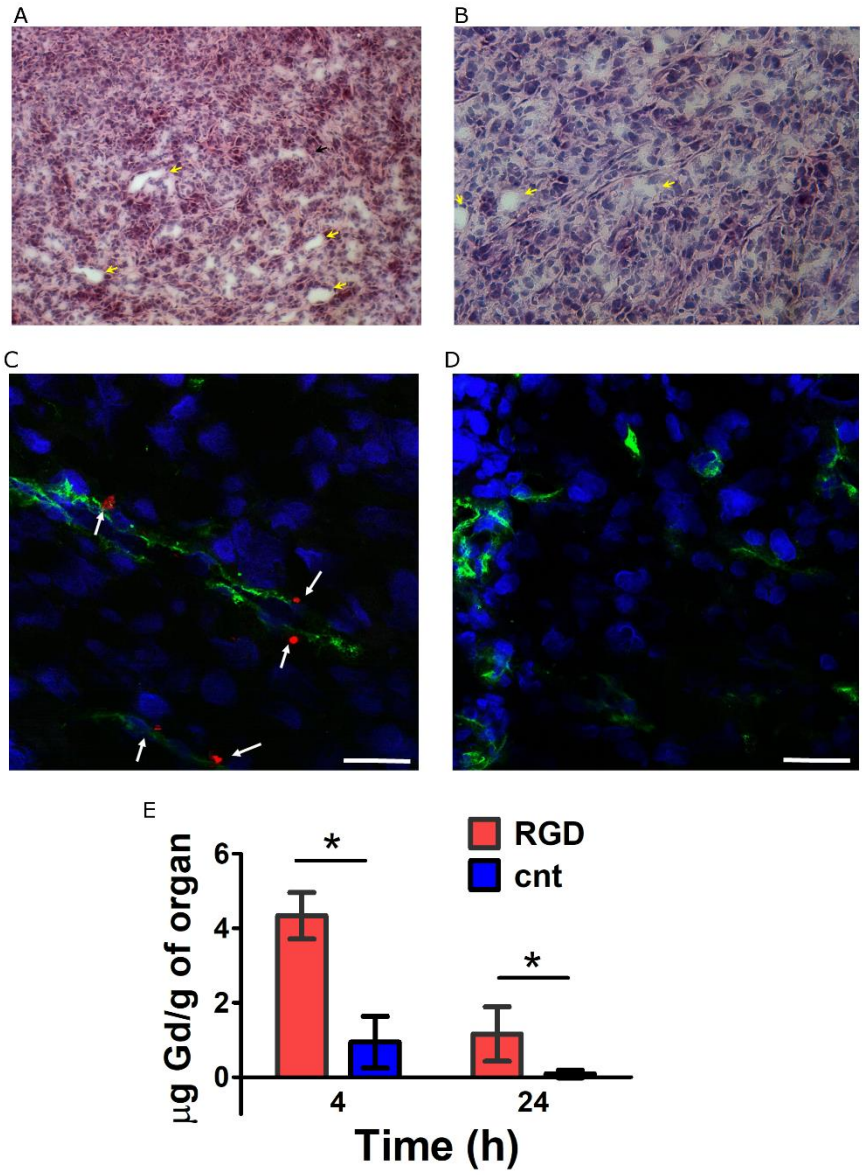

Fig.5. (A,B) H/E histology of representative tumors (10X and 20X, respectively). (C, D) CD-31 fluorescence staining of representative tumors from mice treated with either RGD-Gd GUVs or ctrl-Gd GUVs, respectively. *Green*=Vessels (CD-31/NG-2/CD-105), *Blue*=Nuclei (To-Pro) and *Red*=GUVs (rhodamine). Scale bar=10 µm. (E) ICP-MS quantification of Gd-content in tumors.

After the completion of the MRI experiments, the mice were sacrificed and tumors were explanted for histology and ICP-MS analyses. The H/E staining of the tumors (**Fig.5A, B**) shows homogeneous tumor growth with consistent and regular vascularization (*yellow arrows*) and the absence of necrotic regions. These features were confirmed for all tested tumors. The CD-31 fluorescence staining of the slices showed that the GUVs were only bound to vessels in Group2 mice (*i.e.* those ones treated with RGD-Gd GUVs) (**Fig.5C** *white arrows*), and not those in Group1 (*i.e.* those ones treated with ctrl-Gd GUVs) (**Fig.5D**).

Finally, the quantification of Gd(III) content in the tumors was carried out using the ICP-MS technique. As reported in **Fig. 5E**, the amount of Gd(III) is higher in tumors from Group2 than in those in Group1, both at t=4 h and t=24 h (P-value < 0.05). In Group2 tumors, 4.2 μg Gd/g of tumor and 1.6 μg Gd/g of tumor are present at t=4 h and t=24 h, respectively.

Discussion

The ability to target cancer cells,[2,15] and visualize them using a high resolution imaging technique, such as MRI,[2,4] is one of the most important goals of molecular imaging. Undoubtedly, detecting cancer cells at an early stage by MRI is of huge importance, and will allow the primary role of this diagnostic approach to be further enhanced within the field of oncology.[2] Unfortunately, the intrinsically low sensitivity of MRI means that reaching the detection threshold in targeting experiments is challenging. Many attempts to obtain T_{1w} and/or T_{2w} images of cancer cells upon the administration of targeted contrast agents have been carried out over the last two decades.[4-8,15] The use of T_1 contrast agents has not provided convincing results, especially when targeted epitopes are sparse.[41]

In this work, we have explored a new way to tackle the sensitivity drawbacks of MRI by exploiting the synergy offered by two strategies: *i*) RGD-Containing Giant Unilamellar Vesicles (GUVs); and *ii)* MRI detection based on the assessment of Magnetization Transfer Contrast (MTC) as an

alternative to the commonly used T_{1w} images that are acquired in the presence of paramagnetic GBCAs.[20, 26-28]

GUVs were chosen as they are biocompatible carriers that can be loaded with high payloads of T_1 Gd-based MRI CAs both encapsulated in the large inner cavity and incorporated into the phospholipidic membrane.

The inner cavity was filled with a HEPES/NaCl buffer solution containing 40 mM of Gd-HPDO3A. Although the Gd-HPDO3A dose can be increased up to 300 mM without any osmolarity problems, this did not appear to be convenient because of the occurrence of relaxivity "quenching" upon increasing the amount of entrapped Gd-complexes. This is due to the low water permeability of the GUV membrane.[42-44] For this reason, and in order to increase the attainable relaxivity, the amphiphilic Gd-complex was inserted into the GUV membrane. The Gd-complexes exposed on the outside of the GUVs did not show any drawbacks in their function as agents that shorten the T_1 of water.

The ability to easily functionalize the surfaces of phospholipid vesicles (*e.g.* GUVs, SUVs, micelles, etc.) with targeting moieties is a particular advantage. [23,33] Cyclic RGD has been used, herein, for its binding to integrins. The RGD tripeptide (Arg-Gly-Asp) is an amino acid sequence that is largely present in many extracellular matrix proteins (*e.g.* fibronectin, vitronectin, laminin, etc.) and is responsible for cell-cell and cell-matrix adhesion. This sequence is recognized by a number of integrin proteins, including $\alpha v\beta_3$, $\alpha_5\beta_1$ and $\alpha IIb\beta_3$. There is a large overexpression of integrins on the outer surface of solid tumors, and they play an important role in tumor proliferation, invasiveness and metastasis formation.[45,46]

Furthermore, integrin expression is also increased in endothelial cell surfaces during neo-angiogenesis, to facilitate the growth and survival of newly forming vessels.[47,48]

These liposomes have micrometric diameter (1.5-2 μm) and a slightly negative surface ζ-potential, making them suitable for extravascular/extracellular targeting. No significant differences between RGD-Gd GUVs and ctrl-Gd GUVs were reported. As previously reported,[23] they are only slightly

internalized by macrophages, as observed in *in-vitro* experiments. Furthermore, no evidence of cell toxicity is present in either the targeted or untargeted formulations.

The targeting was efficient and specific. Only in the presence of RGD moiety can the GUV bind integrin-overexpressing cells. It is worth noting that RGD GUVs cannot be internalized by cells, and remain attached to the external surface, although they cluster into specific regions of cytoplasmatic membranes.

The feasibility of using RGD-Gd GUVs for the MRI detection of cancer cells was assessed both *in vitro* and *in vivo* by acquiring T_{1w}, T_{2w} and MTC MR images at 7T.

U-87 MG glioblastoma cells were chosen for the *in-vitro* experiments as they are characterized by a very high expression of RGD receptors, *ca*. 10^5 receptors per cell.[49]

Validation was carried out using fluorescent microscopy and ICP-MS for Gd(III) quantification.

The use of RGD-Gd GUVs allows a very large amount of GBCAs to be carried to the site of interest. This amount is one order of magnitude higher than the amount obtained with the use of ctrl-Gd GUVs (*i.e.* $1.2\text{x}10^8$ *vs.* $8.2\text{x}10^6$ Gd^{3+}/cell), which is, nevertheless, lower than the typical threshold reported for cell detection by T_{1w} MRI. In fact, some years ago, an empirical relationship to relate the threshold for MRI detection to relaxivity (r_{1p}) and the number (N) of Gd-complexes associated to each cell was proposed:[8]

$$\mathrm{N} = {}^{10^9}/_{r_{1\mathrm{p}}}$$

Considering that the r_{1p} of RGD-Gd GUVs at 7 T is lower than 2 $mM^{-1}s^{-1}$, the number of Gd-complexes present in cell pellets, after binding RGD-Gd GUVs onto the external surfaces of cells, is *ca.* 4-5 times lower than the detection threshold. This clearly justifies the absence of detectable T_1 contrast upon the incubation of the U-87 MG cells in the presence of RGD-Gd GUVs. It is likely that T_{1w} images would have reported the targeting of RGD-Gd GUVs at a lower field strength, such as 0.5 T, as the measured r_{1p} value at this field strength was found to be 5.5 $mM^{-1}s^{-1}$. The higher relaxivity observed at 0.5 than at 7T reflects, on the one hand, the important contribution provided by the Gd-

complexes that are exposed on the surface of the liposome's membrane and, on the other, the limited exchange of water molecules across the vesicle's membrane, which leads to the "quenching" of the attainable relaxivity that is associated with the large amount of Gd-HPDO3A in the inner aqueous cavity.[42-44] Although this has not yet been analyzed in detail, it is apparent that water-proton relaxation arises mainly from the exposed Gd-complexes that, being part of a supramolecular and slowly moving system, generate a relaxivity "hump" around a field strength of 1T. The relaxivity of the Gd-GUVs used in this work decreases to lower values as the field strength increases (it is $<2 mM s^{-1}$ at 7T). More work is necessary if the permeability of GUV membranes is to be controlled to take full advantage of the large paramagnetic payload that such systems are capable of delivering.

As expected, better results were obtained by quantifying the T_2 effect. In fact, in this case, cells are detectable upon incubation in the presence of RGD-Gd GUVs, with a ΔR_2 of 18.3% compared to control unlabeled cells. No significant ΔR_2 effect is present in cells upon incubation with ctrl-Gd GUVs.

MRI has traditionally been based on the exploitation of changes in proton density and the T_1 / T_2 relaxation times of tissue water protons. About three decades ago, a new form of tissue contrast was reported; Magnetization Transfer Contrast (MTC). It is based on the concept that tissues contain two, or more, separate populations of water molecules: i) a highly mobile (*free*) water pool; and ii) an immobile, semi-solid (restricted) water pool. This latter is made up of water molecules bound to large macromolecules (*e.g*. ECM proteins, cellular membranes, etc.).

The NMR signal of immobilized water protons is normally not visible because of their very short T_2 relaxation time (bandwidth > 10 KHz). Upon applying *rf* irradiation (at a chemical shift far from the bulk water resonance, with saturation over a very large bandwidth, *e.g.* 50 KHz), the saturated protons may enter the free bulk water proton pool (bandwidth < 20Hz) thus transferring their saturated magnetization to the free water protons. As consequence, there is a decrease in the visible MR signal and consequently the generation of contrast in regions in which the immobilized water molecules/proteins are present.[26-28]

MTC MRI has been widely investigated, at both clinical and preclinical levels, and the intrinsic differences in MTC between tissues have been exploited without the need to administer exogenous CAs.[50,51]

The theoretical relationship between the MTC effect and water T_1 has been widely investigated.[26-28] Our aim is to assess whether this approach is even more sensitive than the usual effects of paramagnetic agents in T_{1w} MR images. In a previous work, we proved that Gd-labelled cells can be detected better by MTC than via the acquisition of T_{1w} images.[20] Our current *in-vitro* experiments on U-87 MG cells have confirmed these previous observations. In fact, cells that were incubated in the presence of RGD-Gd GUVs were detectable by MTC-MRI. In particular, *ca*. 15% contrast difference was observed between the cells incubated with targeted-GUVs and the cells incubated in the presence of ctrl-Gd GUVs. Hence, when T_1 cannot detect U-87 MG cells, MTC succeeds in providing improved sensitivity.

Using the positive *in-vitro* results as a base, we carried out *in-vivo* experiments with the aim of exploring whether the advantages offered by MTC can be translated to *in-vivo* studies.

Mice underwent MRI examination when tumors reached a growth stage in which neo-angiogenesis and epithelial-mesenchymal transition events occur, but when necrotic areas are still not present; the tumors appeared to be well vascularized and perfused.

Analogously to the *in-vitro* experiments, *in-vivo* T_2 and T_1 contrast also failed to distinguish the tumors of mice injected with RGD- and ctrl-Gd GUVs. However, MTC was successful as it detected the pharmacokinetics of the GUVs in the tumor region. The MTC data suggest that the RGD-Gd GUVs were specifically bound to the glioblastoma tumor with a maximum effect around t=4 h (MTC% contrast of *ca*. 16%).

ICP-MS confirmed the specific accumulation of GBCAs, upon use of RGD-Gd GUVs. In fact, the amount of Gd found in the tumors upon the administration of the targeted GUVs is *ca.* 4 and 8 times higher than those of Gd found in tumors upon the administration of control untargeted GUVs (at t=0

and t=4h, respectively). Finally, the CD-31 fluorescence staining of the tumor slices indicated that a significant fraction of the RGD-Gd GUVs was bound to vessels in mice.

It should be noted that the GUVs cannot escape the vascular space *in vivo*, and this means that *in-vitro* and *in-vivo* RGD-targeting experiments are slightly different. In fact, the *in-vitro* experiments demonstrated that RGD GUVs directly bind the RGD that is overexpressed in U-87 MG cells (note that *ca*. 10^5 RGD receptors are present for each U-87 MG cell).[47] Hence, it can be stated that RGD GUVs directly bind tumor cells.

In the *in-vivo* experiments, although the xenografts consisted of U-87 MG glioblastoma cells, the observed MTC effects cannot be associated to GUV's binding of tumor cells as the size of the GUV particles hamper their extravasation from the vascular space. It follows that the observed effect relies on the binding of the integrins that are present on the surface of tumor endothelial cells (TECs). As widely reported in cancer-related literature, integrin expression is strongly increased in endothelial cell surfaces during neo-angiogenesis to facilitate the growth and survival of newly forming vessels. Tumor endothelial cells are markedly different from normal endothelial cells (NECs).[52] This transition from NECs to TECs is triggered by the presence of tumor cells *via* several mechanisms, including: i) transdifferentiation, *i.e*. tumor cells, cancer stem cells or vascular progenitor cells might directly transdifferentiate into TECs; and ii) cell fusion, *i.e*. malignant tumor cells can fuse with NECs or circulating vascular progenitor cells. Both mechanisms lead to the over-expression of integrins on endothelial-cell surfaces.

Altogether, the herein reported data show that a protocol for the efficient detection of integrins that are overexpressed on glioblastoma tumors is possible.

The use of GUVs appears to be a good strategy for the delivery of a high amount of Gd-based MRI contrast agents to the tumor region. They appear to improve the sensitivity threshold of small unilamellar liposomes, while preserving their main advantages. In fact, they are biocompatible and easily loaded with contrast agents, just like as small liposomes, but they are neither sequestered by

macrophages nor internalized inside cells *in vivo*. Moreover, their inner cavity can host a very large number of Gd-complexes.[23] However, although giant liposomes are able to deliver high Gd-complex amounts to the cancer region via the binding of overexpressed integrins, Gd concentration in the region of interest appears to be just at the threshold for the detection of the relaxation enhancement effects using conventional T_{1w} and T_{2w} images.

MTC MRI has been confirmed to possess higher sensitivity for the detection of the small effects that are associated with the presence of paramagnetic Gd-complexes than their $T_{1/2w}$ counterparts.

In conclusion, the synergic properties of applying RGD-Gd GUVs and the MTC-MRI technique have led to the successful visualization of the targeting of tumor integrins. The findings reported herein are promising for the development of new procedures for the preclinical targeting of epitopes that are expressed at low doses on the external surfaces of cells. More generally, the combination of MTC and GBCAs deserves more attention as it is a valid alternative to classical T_{1w} and T_{2w} MRI approaches.

References

1. Bray F, Ferlay J, Soerjomataram I, et al. Global cancer statistics 2018: GLOBOCAN estimates of incidence and mortality worldwide for 36 cancers in 185 countries. CA Cancer J Clin. 2018;68:394-424.
2. Penet MF, Artemov D, Farahani K, Bhujwalla ZM. MR - Eyes for Cancer: Looking Within an Impenetrable Disease. NMR Biomed. 2013; 26: 745-55.
3. Frenzel T, Lawaczeck R, Taupitz M, Jost G, Lohrke J, Sieber MA, Pietsch HL. Contrast Media for X-ray and Magnetic Resonance Imaging: Development, Current Status and Future Perspectives. Invest Rad. 2015; 50:671-678.
4. Wahsner J, Gale EM, Rodríguez-Rodríguez A, Caravan P. Chemistry of MRI Contrast Agents: Current Challenges and New Frontiers. Chem Rev. 2019; 119: 957-1057.
5. Sherry AD, Caravan P, Lenkinski RE. Primer on Gadolinium Chemistry. J Magn Reson Imaging. 2009; 30:1240-8.
6. Geraldes CF, Laurent S. Classification and Basic Properties of Contrast Agents for Magnetic Resonance Imaging Contrast Media Mol Imaging. 2009; 4:1-23.
7. Pierre VC, Allen MJ, Caravan P. Contrast Agents for MRI: 30+ Years and Where Are We Going? J Biol Inorg Chem. 2014; 19: 127-31.
8. Aime S, Cabella C, Colombatto S, Geninatti Crich S, Gianolio E, Maggioni F. Insights Into the Use of Paramagnetic Gd(III) Complexes in MR-molecular Imaging Investigations. J Magn Reson Imaging. 2002; 16:394-406.

9. Le Fur M, Caravan P. The biological fate of gadolinium-based MRI contrast agents: a call to action for bioinorganic chemists. Metallomics, 2019; 11:240-254.
10. Frenzel T, Apte C, Jost G, Schockel L, Lohrke J, Pietsch H. Quantification and Assessment of the Chemical Form of Residual Gadolinium in the Brain After Repeated Administration of Gadolinium-Based Contrast Agents: Comparative Study in Rats. Invest. Rad. 2017; 52:396-404.
11. Di Gregorio E, Ferrauto G, Furlan C, Lanzardo S, Nuzzi R, Gianolio E, Aime S. The Issue of Gadolinium Retained in Tissues: Insights on the Role of Metal Complex Stability by Comparing Metal Uptake in Murine Tissues Upon the Concomitant Administration of Lanthanum- and Gadolinium-Diethylentriamminopentaacetate. Invest. Rad. 2018; 53: 167-172.
12. Di Gregorio E, Furlan C, Atlante S, Stefania R, Gianolio E, Aime S. Gadolinium Retention in Erythrocytes and Leukocytes From Human and Murine Blood Upon Treatment With Gadolinium-Based Contrast Agents for Magnetic Resonance Imaging. Invest. Rad. 2020; 55: 30-37.
13. Strzeminska I, Factor C, Robert P, Grindel AL, Comby PO, Szpunar J, Corot C, Lobinski RL Long-Term Evaluation of Gadolinium Retention in Rat Brain After Single Injection of a Clinically Relevant Dose of Gadolinium-Based Contrast Agents. Invest. Rad. 2020; 55:138-143.
14. Knobloch G, Frenzel T, Pietsch H, Jost G. Signal Enhancement and Enhancement Kinetics of Gadobutrol, Gadoteridol, and Gadoterate Meglumine in Various Body Regions: A Comparative Animal Study. Invest. Rad. 2020; 55:367-373.
15. Strijkers GJ, Kluza E, Van Tilborg GA, van der Schaft DW, Griffioen AW, Mulder WJ, Nicolay K. Paramagnetic and Fluorescent Liposomes for Target-Specific Imaging and Therapy of Tumor Angiogenesis Angiogenesis. 2010; 13:161-73.
16. Man F, Lammers T, T M de Rosales R. Imaging Nanomedicine-Based Drug Delivery: A Review of Clinical Studies. Mol Imaging Biol. 2018; 20: 683-695.
17. Torchilin V. P., Weissig V., in Liposomes: Practical Approach, Oxford University Press, NY, USA, 2nd ed., 2003, pp. 4-7
18. Chan KW, Bulte JW, McMahon MT. Diamagnetic Chemical Exchange Saturation Transfer (diaCEST) Liposomes: Physicochemical Properties and Imaging Applications Wiley Interdiscip Rev Nanomed Nanobiotechnol. 2014; 6:111-24.
19. Jia Y, Geng K, Cheng Y, Li Y, Chen Y, Wu R. Nanomedicine Particles Associated With Chemical Exchange Saturation Transfer Contrast Agents in Biomedical Applications. Front Chem. 2020; 8:326.
20. Delli Castelli D, Ferrauto G, Di Gregorio E, Terreno E, Aime S. Sensitive MRI detection of internalized T1 contrast agents using magnetization transfer contrast. NMR Biomed. 2015; 28:1663-70.
21. Zhao JM, Har-el YE, McMahon MT, Zhou J, Sherry AD, Sgouros G, Bulte JW, van Zijl PC. Size-induced Enhancement of Chemical Exchange Saturation Transfer (CEST) Contrast in Liposomes J Am Chem Soc. 2008; 130:5178-84.
22. Morales-Penningston NF, Wu J, Farkas ER, Goh SL, Konyakhina TM, Zheng JY, Webb WW, Feigenson GW. GUV Preparation and Imaging: Minimizing Artifacts Biochim Biophys Acta. 2010; 1798:1324-32.
23. Tripepi M, Ferrauto G, Bennardi PO, Aime S, Delli Castelli D. Multilamellar LipoCEST Agents Obtained From Osmotic Shrinkage of Paramagnetically Loaded Giant Unilamellar Vescicles (GUV). Angewandte Chemie Int. Ed. 2020; 59:2279-2283
24. Ferrauto G, Delli Castelli D, Di Gregorio E, Terreno E, Aime S. LipoCEST and cellCEST Imaging Agents: Opportunities and Challenges Wiley Interdiscip Rev Nanomed Nanobiotechnol. 2016; 8: 602-18.

25. Langereis S, Geelen T, Grüll H, Strijkers GJ, Nicolay K. Paramagnetic liposomes for molecular MRI and MRI-guided drug delivery. NMR Biomed. 2013;26:728-44.
26. Henkelman RM, Stanisz GJ, Graham SJ. Magnetization transfer in MRI: a review. NMR Biomed. 2001;14:57–6.
27. Knutsson L, Xu J, Ahlgren A, van Zijl PCM. CEST, ASL, and Magnetization Transfer Contrast: How Similar Pulse Sequences Detect Different Phenomena. Magn Reson Mad. 2018: 80: 1320–1340.
28. Van Zijil PCM, Yadav NN. Chemical Exchange Saturation Transfer (CEST): What Is in a Name and What Isn't? Magn Res Med. 2011; 65:927-48.
29. Ferrauto G, Aime S, McMahon MT, Morrow JR, Snyder EM, Li A, Bartha R. Chapter 3 –pp. 243-317-Contrast Agents for MRI: Experimental Methods Editors. Edited by Pierre VP, Allen MJ. RSC.
30. Runge VM. Safety of Approved MR Contrast Media for Intravenous Injection J Magn Reson Imaging. 2000; 12:205-13.
31. Anelli PL, Lattuada L, Lorusso V, Schneider M, Tournier H, Uggeri F, Mixed Micelles Containing Lipophilic Gadolinium Complexes as MRA Contrast Agents. MAGMA. 2001; 12: 114-120.
32. Barge A, Cravotto G, Gianolio E, Fedeli F. How to Determine Free Gd and Free Ligand in Solution of Gd Chelates A Technical Note. Contrast Media Mol Imaging. 2006;1: 184-8.
33. Reeves J P, Dowben R M. Formation and properties of thin-walled phospholipid vesicles. Journal of cellular physiology.1969; 73: 49-60.
34. Mulas G, Ferrauto G, Dastru W, Anedda R, Aime S, Terreno E. Insights on the relaxation of liposomes encapsulating paramagnetic Ln-based complexes. Magn.Res. Med.. 2015; 74: 468-473.
35. Reulen SWA, Brusselaars WWT, Langereis S, Mulder WJM, Breurken M, Merks M. Protein-liposome Conjugates Using Cysteine-Lipids and Native Chemical Ligation. Bioconjug Chem.2007; 18,590-6
36. Riss Tl, Moravec RA, Niles Al, Duellman S, Benink HA, Worzella TJ, Minor L. Cells viability assays. Sittampalam GS, Grossman A, Brimacombe K, et al., editors. Bethesda (MD): Eli Lilly & Company and the National Center for Advancing Translational Sciences; 2004-
37. Ferrauto G, Di Gregorio E, Auboiroux V, Petit M, Berger F, Lahrech H. CEST-MRI for Glioma pH Quantification in Mouse Model: Validation by Immunohistochemistry. NMR biomed. 2018; 31:e4005.
38. Ferrauto G, Di Gregorio E, Lanzardo S, Ciolli L, Iezzi M, Aime S. Generation of Multiparametric MRI Maps by Using Gd-labelled- RBCs Reveals Phenotypes and Stages of Murine Prostate Cancer. Sci. Rep. 2018; 8:10567.
39. Ferrauto G, Di Gregorio E, Delli Castelli D, Aime S CEST-MRI studies of cells loaded with lanthanide shift reagents. Magn Reson Med. 2018; 80:1626-1637.
40. Ferrauto G, Delli Castelli D, Terreno E, Aime S. Magn Reson Med. 201; 69 :1703-11.
41. Lanza G;. Winter PM, Neubauer AM, Caruthers SD, Hockett FD, Wickline SA. 1H/19F Magnetic Resonance Molecular Imaging With Perfluorocarbon Nanoparticles. Curr Top Dev Biol. 2005; 70:57-76.
42. Strijkers GJ , Hak S, Kok MB, Springer CS, Nicolay K, Three-compartment T1 relaxation model for intracellular paramagnetic contrast agents. Magn Reson Med. 2009; 61:1049–105.
43. Guenoun J, Doeswijk GN, Krestin GP, Bernsen MR. Compartmentalization of Gd liposomes: the quenching effect explained Contrast Media Mol Imaging 2016;11:106-14.
44. Di Gregorio E, Ferrauto G, Gianolio E, Aime S Gd loading by hypotonic swelling: an efficient and safe route for cellular labeling. Contrast Media Mol Imaging. 2013; 8: 475-86.
45. Hamidi H, Pietila M, Ivaska J. The complexity of integrins in cancer and new scopes for therapeutic targeting. Br J Cancer. 2016; 115: 1017–1023.

46. Sokeland G, Schumacher U. The functional role of integrins during intra- and extravasation within the metastatic cascade. Mol Cancer. 2019; 18: 12.
47. Weis SM, Cheresh DA. αv Integrins in Angiogenesis and Cancer Cold Spring Harb Perspect Med. 2011; 1:A006478
48. Avraamides CJ, Garmy-SUsini B, Varner JA. Integrins in angiogenesis and lymphangiogenesis Nat Rev Cancer. 2008 Aug; 8(8): 604–617.
49. Zhang X, Xiong Z, Wu Y, Cai W, Tseng YR, Gambhir SS, Chen X. Quantitative PET Imaging of Tumor Integrin αvβ3 Expression with 18F-FRGD2 J Nucl Med. 2006; 47: 113–121.
50. Mehta RC, Pike GB, Enzmann DR. Magnetization transfer magnetic resonance imaging: a clinical review. Top Magn Reson Imaging. 1996;8 :214-30.
51. Maas MC, Litjens GJS, Wright AJ, Attenberger UI, Haider MA, Helbich TH, Kiefer B, Macura KJ, Margolis DJA, Padhani AR, Selnæs KM, Villeirs GM, Fütterer JJ, Scheenen TWJ A Single-Arm, Multicenter Validation Study of Prostate Cancer Localization and Aggressiveness With a Quantitative Multiparametric Magnetic Resonance Imaging Approach. Invest Radiol. 2019; 54: 437-447.
52. Hida K, Maishi N, Annan DA, Hida Y. Contribution of Tumor Endothelial Cells in Cancer Progression. Int J Mol Sci. 2018; 19: 1272.